Applied Catalysis B: Environmental 190 (2016) 12–25

Contents lists available at ScienceDirect

Applied Catalysis B: Environmental

journal homepage: www.elsevier.com/locate/apcatb

Small-sized Ni(1 1 1) particles in metal-organic frameworks with low over-potential for visible photocatalytic hydrogen generation

Wenlong Zhen[a,b], Jiantai Ma[b], Gongxuan Lu[a,*]

[a] State Key Laboratory for Oxo Synthesis and Selective Oxidation, Lanzhou Institute of Chemical Physics, Chinese Academy of Sciences, Lanzhou, China
[b] College of Chemistry and Chemical Engineering, Lanzhou University, Lanzhou, China

ARTICLE INFO

Article history:
Received 23 September 2015
Received in revised form 6 January 2016
Accepted 25 February 2016
Available online 28 February 2016

Keywords:
Small-sized Ni(1 1 1) particles
Metal-organic frameworks
Low over-potential
Visible photocatalytic hydrogen generation

ABSTRACT

The development of an advanced co-catalyst is critical for improving the efficiency of the photocatalytic hydrogen evolution reaction. Noble metals (such as Pt) have been identified to be the most active co-catalyst for this reaction since they exhibit significantly low over-potential. However, their low-abundance, high cost, its scale-up setup usage is impeditive. Here, we reported that high efficient small-sized nickel particles embedded in the frameworks of MOF-5 as a co-catalyst with low over-potential for visible photocatalytic hydrogen evolution. The electrochemical measurements showed a low over-potential of −0.37 V, which have the similar over-potential as Pt@MOF-5. Such low over-potential is attributed to their high dispersion (41.8%), small-sized nickel particles (~9 nm), and high specific surface area of MOF-5 (2973 m^2/g). As evidenced by electrochemical impedance spectra (EIS) measurements, Ni nanoparticles with exposed (1 1 1) facet were more benefited the electrons transfer from MOF-5 than that of (2 0 0) facet one. In addition, Ni@MOF-5 exhibited the larger transient photocurrent and longer fluorescence lifetime. These results led to the high photocatalytic activities and stability for hydrogen evolution sensitized by Eosin Y (EY) over Ni@MOF-5. The rate of hydrogen evolution reached 30.22 mmol h^{-1} $g^{-1}_{[Ni]}$ (at pH 11) over Ni@MOF-5 irradiated under visible light irradiation ($\lambda \geq 420$ nm) in 2 h. The apparent quantum efficiency (AQE) of 16.7% over EY-Ni@MOF-5 was achieved at 430 nm. MOF-5 might promote the photogenerated electrons transfer from excited EY to the hydrogen evolution active sites (Ni), and consequently enhance photocatalytic hydrogen evolution efficiency.

1. Introduction

Hydrogen is being vigorously pursued as a future energy carrier in the transition from the fossil energy to renewable energy for our society [1]. Sustainable hydrogen production from water splitting has attracted growing attentions [2–4]. In particular, the photocatalytic hydrogen evolution reaction (HER) efficiency significantly relies on the properties of the hydrogen evolution co-catalysts that reduce the over-potential of HER. The most effective HER co-catalysts are Pt-group metals [4], since they are active and have low over-potential for H_2 production from water [5–7]. However, the scale-up application of the Pt-based catalysts is still difficult because of their scarceness and high-cost. It is therefore urgently to develop new non-noble metal hydrogen evolution co-catalysts which are highly active, stable, low-cost and possess low over-potential of HER [8].

Ni is a typical active co-catalyst for hydrogen evolution, however, unlike noble metal; Ni particles are easily to aggregate to large diameter domain, thus leads to low dispersion and activity. In order to achieve the goal of fabrication of high active Ni center, the difficulty of confinement of stable Ni particle in the substrates must be solved. Usually, it is quite difficult to load enough active species over low specific area supports, although several techniques have been explored, such as multi-impregnation with a low concentration of salt [9], different precursors [10], different pH values [11] and addition of alkaline elements as anchor connecting components [12]. In the past few years, metal-organic frameworks (MOFs), with a feature of three-dimensional (3D) framework structure, are potential candidates for catalysts and catalyst supports [13–16]. Due to their extremely large surface area of ~2900m^2 g^{-1}, well-ordered porous structures and channels, and diverse means available for post-synthesis functionalization, MOFs have been used for gas storage or separation [17–20], drug-delivery [21,22] and catalysis [23–25]. Although there are still some limitations, the possibilities for MOFs as heterogeneous catalysts are very encouraging [16,26–30]. For example, D. Sun et al. reported NH_2-MIL-125(Ti)

* Corresponding author.
E-mail address: gxlu@lzb.ac.cn (G. Lu).

http://dx.doi.org/10.1016/j.apcatb.2016.02.061
0926-3373/

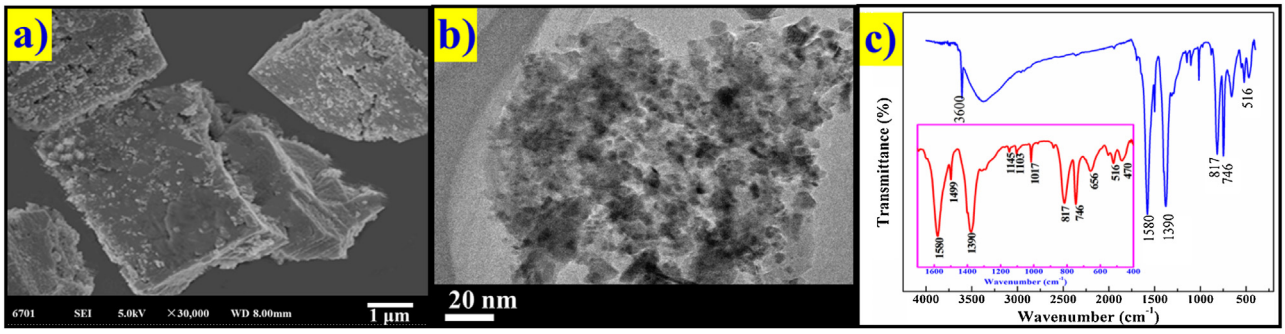

Fig. 1. SEM (a), TEM (b) and FT-IR (c) images of pure MOF-5.

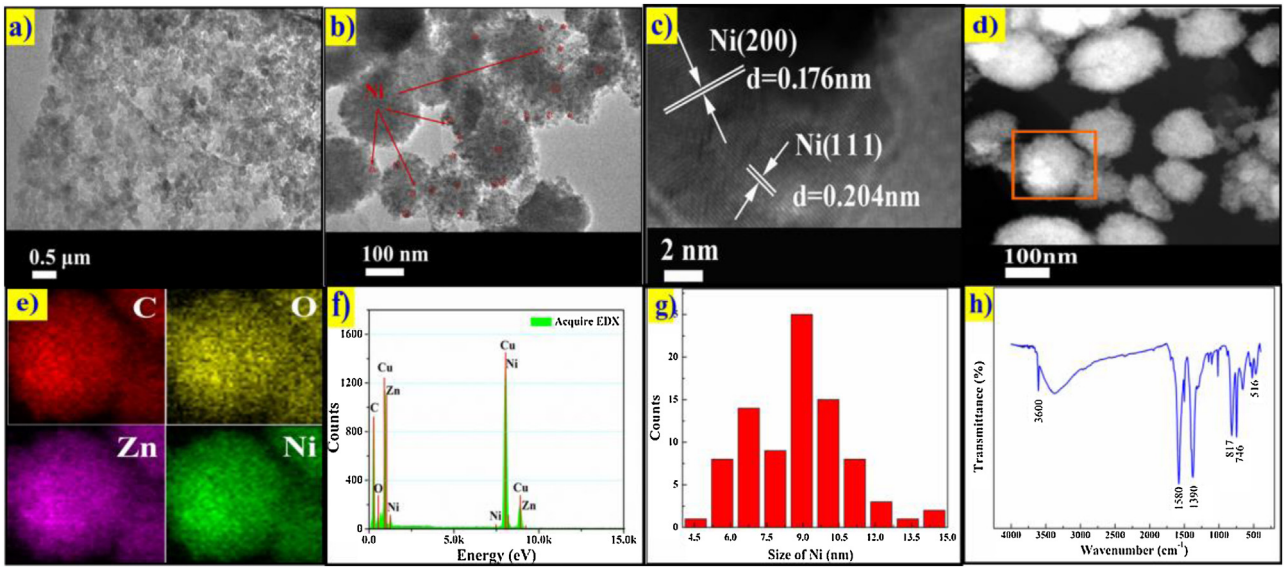

Fig. 2. TEM (a–b), HRTEM (c), HAADF-STEM (d), EDX elemental mapping (e), EDX spectrum (f), particle size distribution of Ni (g) and FT-IR images of Ni@MOF-5 (h).

exhibited excellent photocatalytic performance for the aerobic oxidation of amine to imine [31], and NH_2-MIL-125(Ti) can photocatalytic reduce CO_2 to form formate under visible light [32]. Wang et al. synthesized Fe-based MOF materials showed photocatalytic activity for CO_2 reduction under visible light irradiation in the presence of TEOA as a sacrificial agent [33]. Horiuchi et al. prepared the amino-functionalized Ti(IV) MOF (Ti-MOF-NH_2), and found to photocatalyze efficiently the hydrogen production reaction in an aqueous solution containing TEOA as a sacrificial electron donor under visible light irradiation conditions [34]. In addition, MOFs was found to be photoactive, and photon induced charge separation was observed in MOF-5 [35]. Its 3D channel structure also offered paths for effective charge collection and transport [36]. Therefore, it is possible to prepare a non-noble metal catalyst (such as Ni) with low over-potential for HER, if high-dispersed and small-sized nanoparticles (NPs) embedded on MOFs is accomplished.

Dye sensitized photocatalysts typically comprises of a metal complex photosensitizer (PS), *e.g.*, Eosin Y (EY) for solar light harvesting and a metal based co-catalyst, such as metallic colloidal Ni or Ni-complexes for reduction of proton by electrons from the excited PS directly or *via* electron transfer. Dye-sensitized photocatalytic hydrogen generation systems offer the catalyst ability using longer wavelength visible light in a majority of the solar spectrum [37–42].

Herein, high efficient co-catalyst, small-sized nickel particles anchored in the frameworks of MOF-5 (Ni@MOF-5) with low overpotential for photocatalytic hydrogen evolution was reported. Very high dispersion of Ni (41.8%) over MOF-5 (2973 m^2/g) has been achieved. Ni@MOF-5 shows the larger transient photocurrent and longer fluorescence lifetime. The small-sized Ni co-catalyst showed low over-potential similar to Pt@MOF-5 for HER. Ni particles with exposed (1 1 1) facets in MOF-5 exhibited higher activity than that of (2 0 0) facets. After sensitized by EY, the highest apparent quantum efficiency was accomplished under 430 nm illuminations over Ni@MOF-5. MOF-5 promoted the photogenerated electrons transfer from excited EY to small-sized Ni particles, the hydrogen evolution active sites, and consequently enhanced visible photocatalytic hydrogen generation efficiency. The Ni@MOF-5 catalyst could be a promising substitute for noble-metals in photocatalytic hydrogen generation.

2. Experimental

2.1. Materials

Zinc nitrate hexahydrate ($Zn(NO_3)_2{\cdot}6H_2O$, AR, Xilong Chemical Co., Ltd.), Nickel(II) acetylacetonate ($Ni(acac)_2$, AR, J&K Scientific Ltd.), Potassium platinic chloride (K_2PtCl_6, 99%, Nanjing Chemlin Chemical Co., Ltd.), *N*,*N*-dimethylformamide (DMF, 99.5%, Xilong Chemical Co., Ltd.), terephthalic acid (H_2BDC, ≥99.0%, Shanghai KEFENG Chemical Reagent Co., Ltd.), acetone (AR, Xilong Chemical Co., Ltd.), hydrazine solution ($N_2H_4{\cdot}H_2O$, AR, Tianjin NO.2 Reagent Co., Ltd.), Silica (SiO_2, 40 mesh, Shanghai Meryer Chemical Technology Co., Ltd.), Ethanol (C_2H_5OH, AR, Xilong Chemical Co.,

Ltd.), Mesitylene (98% Sigma-Aldrich), Hexadecylamine (90% HDA, Aldrich), Trioctylphosphine (TOP, 90% Sigma-Aldrich), Toluene ($C_6H_5CH_3$, AR, Xilong Chemical Co., Ltd.), Oleic acid ($C_{18}H_{34}O_2$, 99%, J&K Scientific Ltd.), Oleyl amine ($C_{18}H_{37}N$, 85%, Shanghai KEFENG Chemical Reagent Co., Ltd.), Octadecene ($C_{18}H_{36}$, 97%, J&K Scientific Ltd.), Iron(0) pentacarbonyl (Fe(CO) 5, J&K Scientific Ltd.), Cyclohexane (C_6H_{12}, AR, Tianjin NO.2 Reagent Co. Ltd.), Hexanes (C_6H_{14}, AR, Tianjin NO.2 Reagent Co., Ltd.).

2.2. Catalysts preparation

2.2.1. Synthesis of MOF-5

MOF-5 was synthesized by the solvent-thermal route according to the previous literature [15,43]. In a glass reactor equipped with a reflux condenser and a teflon-lined stirrer, 1.025 g of H_2BDC and 4.825 g of $Zn(NO_3)_2{\cdot}6H_2O$ were dissolved in 148.9 mL of DMF and heated up to 130 °C for 4 h. After about 45 min, crystallization started and the formerly clear solution turned slightly opaque. After 4 h, the reaction product was cooled down to room temperature. The solid was filtered off, washed three times with 100 mL of dry acetone and dried under a stream of nitrogen. Finally, as-synthesized MOF-5 was calcinated in N_2 flow at 250 °C for 6 h to remove the guest molecules from the pores.

2.2.2. Synthesis of Ni particles

The co-catalyst Ni particles were prepared by reduction methods. $Ni(acac)_2$ (4 g) was dissolved in ethanol (30 mL) to form a dark green solution at room temperature. Subsequently, 10 mL of hydrazine solution, 10 g of NaOH and distilled water (10 mL) were added into the solution under continuous agitation. The mixture was stirred until no longer produces bubbles. The obtained dispersions were filtered, washed with water several times. Finally, the obtained wet solids were dried at 80 °C for 5 h.

2.2.3. Synthesis of Ni@MOF-5 and Pt@MOF-5.

Ni@MOF-5 catalysts was prepared by impregnation methods using $Ni(acac)_2$ and MOF-5. $Ni(acac)_2$ (0.875 g) was dissolved in ethanol (150.0 mL) to form a dark green solution at 60 °C. Subsequently, guest-free MOF-5 (1.8 g) was added into the solution under continuous agitation. The mixture was stirred for 16 h in air, and 5.00 mL of hydrazine solution (80 wt%) was added into the aqueous dispersions. The mixture was maintained at this temperature for 8 h until the color of the solution changed into dark. After the reduction was completed, the obtained dispersions were filtered, washed with water several times to remove the impurities. Finally, the obtained wet solids were dried at 110 °C for 12 h and calcined at 250 °C for 5 h under inert atmosphere (N_2). The Ni@MOF-5 catalyst was synthesized and denoted as Ni@MOF-5, the loading of Ni was 10%. The preparation method of Pt@MOF-5 is similar to the method of Ni@MOF-5. K_2PtCl_6 was used as precursor and the loading of Pt was 10%.

2.2.4. Synthesis of nano-cubes structure of Ni(2 0 0) [44]

For a typical synthesis process, 0.3 mmol (0.083 g) of $Ni(acac)_2$, 10 molar equivalents hexadecylamine, and 1 molar equivalents trioctylphosphine were dissolved in 5 mL mesitylene in a 10 mL bottle. The solution was degassed under vacuum, and the atmosphere was replaced with nitrogen, then the bottle was placed inside the Fischer-Porter bottle, and was further degassed under vacuum and finally filled with 1 bar hydrogen. The Fischer-Porter bottle was degassed and refilled with hydrogen twice and then remained the pressure at 1 bar. That Fischer-Porter bottle was transferred into the oven and the temperature was maintained at 140 °C for another 24 h. After that, the Fischer-Porter bottle was removed from the oven and allowed it to cool down to room temperature and then the bottle was released to air. The nanoparticles were separated from the solution using a magnet for a period of 10 min, and then the solution was removed. Toluene was added to make particles re-dispersed in a sonicator. This process was repeated twice more, leaving only the nanocubes remained. The nickel nanoparticles were flocculated with ethanol and were cleaned with a 50:50 mixture of ethanol and toluene *via* centrifugation of 14,000 rpm for 10 min. This process was repeated 5 times. The obtained nanoparticles were redispersed in hexanes.

2.2.5. Synthesis of nano-triangular structure of Ni(1 1 1) [45]

Typically, a slurry containing $Ni(acac)_2$ (1.8 mmol), oleic acid (4 mmol), oleyl amine (16 mmol), and octadecene (10 mL) in a three-necked flask (100 mL) was heated at 373 K to remove water and oxygen, with vigorous magnetic stirring under vacuum for 30 min in a temperature-controlled reactor. The solution was then heated in nitrogen at 473 K, then 0.05 mL $Fe(CO)_5$ dissolved in 2 mmol octadecene was slowly injected into the three-necked flask with a syringe in 3 min. The reaction mixture was kept at 473 K for 20 min. After the reaction system was cooled down to room temperature, the product was centrifuged and washed with cyclohexane once and then with ethanol for three times to remove the solvent and excess surfactants. The nanoparticles were redispersed in hexanes.

2.2.6. Synthesis of nano-hexagonal structure of Ni(1 1 1/2 0 0) [46]

In a typical synthesis route, $Ni(acac)_2$ (2.00 g, 7.80 mmol) was added to 78.0 mmol of oleylamine (20.8 g, 10 equiv). The mixture was degassed at 100 °C and then heated at 220 °C for 2 h under inert atmosphere, giving a black solution. The mixture was cooled down to room temperature and centrifuged after addition of 40 mL of acetone to give a black product. The nanoparticles were redispersed in hexanes.

2.2.7. Loading different exposed facets of Ni NPs on MOF-5 samples [47]

Ni NPs with different exposed facets were embedded on MOF-5 frameworks by a wet-absorption process as follows: (1) in a 50 mL of deionized water, a certain amount of as-prepared Ni NPs were added and ultrasonicated for 10 min; (2) MOF-5 was dispersed into above mentioned Ni NPs dispersion under ultrasonication condition and kept stirring for 24 h; (3) the mixture was filtered and washed three times with deionized water and methanol, dried and finally annealed at 423 K for 2 h. The obtained products were labeled according to the used Ni NPs as Ni(2 0 0)@MOF-5, Ni(2 0 0/1 1 1)@MOF-5, and Ni(1 1 1)@MOF-5, respectively. The loading amount of Ni for all three samples was 1.0%.

2.2.8. Synthesis different sizes (3 and 6 nm) Ni NPs over Ni@MOF-5 [48]

The Ni(3 nm)@MOF-5 catalyst was prepared by the precipitation-deposition method. Firstly, MOF-5 1.8 g was added into ethanol (150.0 mL) under stirring. Then the pH of the resulting suspension was adjusted to 8.0 with $NH_3{\cdot}H_2O$ aqueous solution (0.1 M). Subsequently, 0.875 g $Ni(acac)_2$ aqueous solution (20 mL) was added dropwise into the above suspension and the resulting green suspension was aged at room temperature for 3 h with stirring. The precipitation obtained was separated by centrifugation, washed with water three times and dried at 110 °C for 4 h, followed by calcination in nitrogen at 300 °C for 3 h with a heating rate of 5 °C min^{-1} and the obtained sample was denoted as NiO@MOF-5. Finally, all of the as-calcined NiO@MOF-5 samples were reduced in a gaseous mixture of H_2 and N_2 (2:3, v/v) for 4 h at 300 °C with a heating rate of 5 °C min^{-1}, and the obtained catalysts was denoted as Ni(3 nm)@MOF-5.

The Ni(6 nm)@MOF-5 catalyst was also prepared by the conventional impregnation method. Typically, MOF-5 1.8 g was added to a

0.875 g Ni(acac)$_2$ aqueous solution (5 mL) solution. After agitation for 3 h, the resultant slurry was dried at 110 °C for 4 h, followed by calcination in nitrogen at 300 °C for 3 h. Finally, the sample was reduced in a gaseous mixture of H_2 and N_2 (2:3, v/v) at 300 °C for 4 h with a heating rate of 5 °C min^{-1}, which was denoted as Ni(6 nm)@MOF-5.

Synthesis of Ni(20 nm)@MOF-5 catalyst: First, 20 nm Ni NPs were obtained by the thermolysis of 0.5 mmol Ni(acac)$_2$ solved in 40 mL OA at 215 °C for 30 min in a N_2 atmosphere [49] The reaction mixture turned black, resulting from the nucleation and growth of nickel nanocrystals. Then the solution was removed from oil bath and cooled to room temperature naturally. The nanocrystals were separated upon the addition of equal volume alcohol, centrifuged, and washed using a mixture of alcohol solvent. The Ni NPs were dispersed in hexanes. Subsequently, 20 nm Ni NPs were embedded on MOF-5 frameworks by a wet-absorption process as follows: (1) in a 50 mL of alcohol, as-prepared Ni NPs (10 mg) was added and ultrasonicated for 10 min; (2) 90 mg MOF-5 was dispersed into above mentioned Ni NPs dispersion under ultrasonication condition and kept stirring for 24 h; (3) the mixture was filtered and washed three times with deionized water and methanol, dried and finally annealed at 423 K for 2 h. The obtained product was denoted as Ni(20 nm)@MOF-5.

2.3. Activities measurement

Measurements of photocatalytic H_2 evolution activity were performed in a sealed Pyrex flask (187 mL) with a flat window (an efficient irradiation area of 10.2 cm^2) and a silicone rubber septum for sampling. 50 mg of Ni@MOF-5 and 70 mg of Eosin Y were dispersed into 100 mL of triethanolamine (TEOA)-H_2O solution (10%, v/v, pH 11) under the ultrasound treatment (25 kHz, 250 W) about 10 min. Prior to irradiation, the reactant mixture was degassed by bubbling Ar gas for 40 min.

The light source was a 300-W Xenon lamp with a 420 nm cutoff filter. The amount or rate of hydrogen evolution was measured using gas chromatograph (Aglient 6820, TCD, 13 X columns, Ar carrier). The apparent quantum efficiency (AQE) was measured under the same photocatalytic reaction conditions with irradiation light through a bandpass filter (430, 460, 490, 520, or 550 nm). Photon flux of the incident light was determined using a Ray virtual radiation actinometer (FU 100, silicon ray detector, light spectrum, 400–700 nm; sensitivity, 10–50 μV μm mol^{-1} m^{-2} s^{-1}). The reaction solutions were irradiated for 60 min with bandpass filters for AQE tests on the H_2 production. The following equation was used to calculate the AQE.

$$\mathrm{AQE} = \frac{2 \times \text{the number of evolved hydrogen molecules}}{\text{the number of incident photons}} \times 100\%$$

2.4. Electrochemical measurements

All the electrochemical measurements were measured on an electrochemical analyzer (CHI660A) in a homemade standard three-electrode cell. The working electrodes were prepared by drop-coating sample suspensions directly onto the precleaned indium tin oxide glass (ITO glass) surface. Platinum foil was used as the counter electrode and a saturated calomel electrode (SCE) as the reference electrode. The supporting electrolyte was 10% (v/v) TEOA mixed 0.1 mol/L Na_2SO_4 aqueous solution. The surface area of the working electrode exposed to the electrolyte was about 0.95 cm^2. The cathodic polarization curves were obtained using the linear sweep voltammetry (LSV) technique with a scan rate of 1 mV s^{-1}. For the preparation of working electrodes for photoelectrochemical measurements, 500 μL of EY aqueous solution (1.0×10^{-3} mol/L) was added onto the above catalyst film electrode surface and then dried. A 300-W Xe lamp equipped with an optical cutoff filter of 420 nm was used for excitation.

2.5. Characterization of the catalysts

The X-ray diffraction patterns (XRD) of the samples were recorded on a Rigaku B/Max-RB X-ray diffractometer with a nickel-filtrated Cu Kα radiation over a 2θ range of 15–85° and a position sensitive detector using a step size of 0.017° and a step time of 15 s at 40 mA and 40 kV. X-ray photoelectron spectroscopy (XPS) analysis was performed using a VG Scientific ESCALAB 250Xi-XPS photoelectron spectrometer with an Al Kα X-ray resource. The binding energies were calibrated by the C1s binding energy of 284.7 eV. The specific surface areas (SSA) of the catalysts were determined by N_2 adsorption-desorption measurements by employing the Brunauer-Emmet-Teller (BET) method (Micromeritics apparatus ASAP 2020 M) at 77 K. Transmission electron microscopy (TEM) and HRTEM images were taken with a Tecnai-G2-F30 field emission transmission electron microscope operating at accelerating voltage of 300 kV. UV–vis absorption spectra were obtained with a Hewlett-Packard 8453 spectrophotometer. Fourier transform infrared (FT-IR) spectra were performed on a Nicolet Nexus 870 with the wave number from 4000 to 400 cm^{-1}. The dispersion was measured by H_2 chemisorption using a Micromeritics Chemisorb 2750 Pulse Chemisorption System at 25 °C.

3. Results and discussion

3.1. TEM and FT-IR analysis

MOF-5 was synthesized by the solvent-thermal route according to the previous literature [15,43]. Fig. 1a and b shows the scanning electron microscopy (SEM) and transmission electron microscopy (TEM) images of the pure MOF-5. The images indicate cubic morphology for the prepared crystals of MOF-5, which is similar to the results of previous reports [15,50,51]. The FT-IR results (Fig. 1c) show peaks around 1390 and 1580 cm^{-1} which are due to —C═O in the MOF-5. The peak around 3600 cm^{-1} could be assigned to absorbed water [52,53]. The peaks at 516, 746 and 817 cm^{-1} could be assigned to absorption of H_2BDC.

The typical TEM images and Fourier-transform infrared spectroscopy (FT-IR) spectra of the Ni@MOF-5 samples are shown in Fig. 2. The size dimension of Ni particles over MOF-5 was around 9 nm (shown in Fig. 2a–b). Analysis of high-resolution transmission electron microscopy (HRTEM) images of the Ni nanoparticles (NPs) indicated that the *d*-spacing between two adjacent lattice planes were about 0.204 and 0.176 nm (Fig. 2c). These values were in good agreement with the spacing of Ni (1 1 1) and (2 0 0) planes of face-centered cubic Ni. The high-angle annular dark field scanning transmission electron microscopy (HAADF-STEM) images and energy-dispersive X-ray (EDX) elemental mapping of Ni@MOF-5 clearly indicated that the distribution of Ni, Zn, C and O elements were relatively homogeneous in Ni@MOF-5 (Fig. 2d–e). The EDX measurement also confirmed the existence of Ni, Zn, C and O elements in Ni@MOF-5 (Fig. 2f). The particle size distribution of Ni particles in Ni@MOF-5 catalysts derived from TEM for (Fig. 2g) identified that the main crystallite size of Ni over Ni@MOF-5 catalyst was around 9 nm. The expected strong characteristic absorptions for the symmetric and asymmetric vibrations of BDC (1580 and 1390 cm^{-1}) and absorption water (3600 cm^{-1}) were observed in typical FT-IR spectra of the Ni@MOF-5 given in Fig. 2h [52,53]. The peaks at 516, 746 and 817 cm^{-1} could be assigned to absorption of H_2BDC.

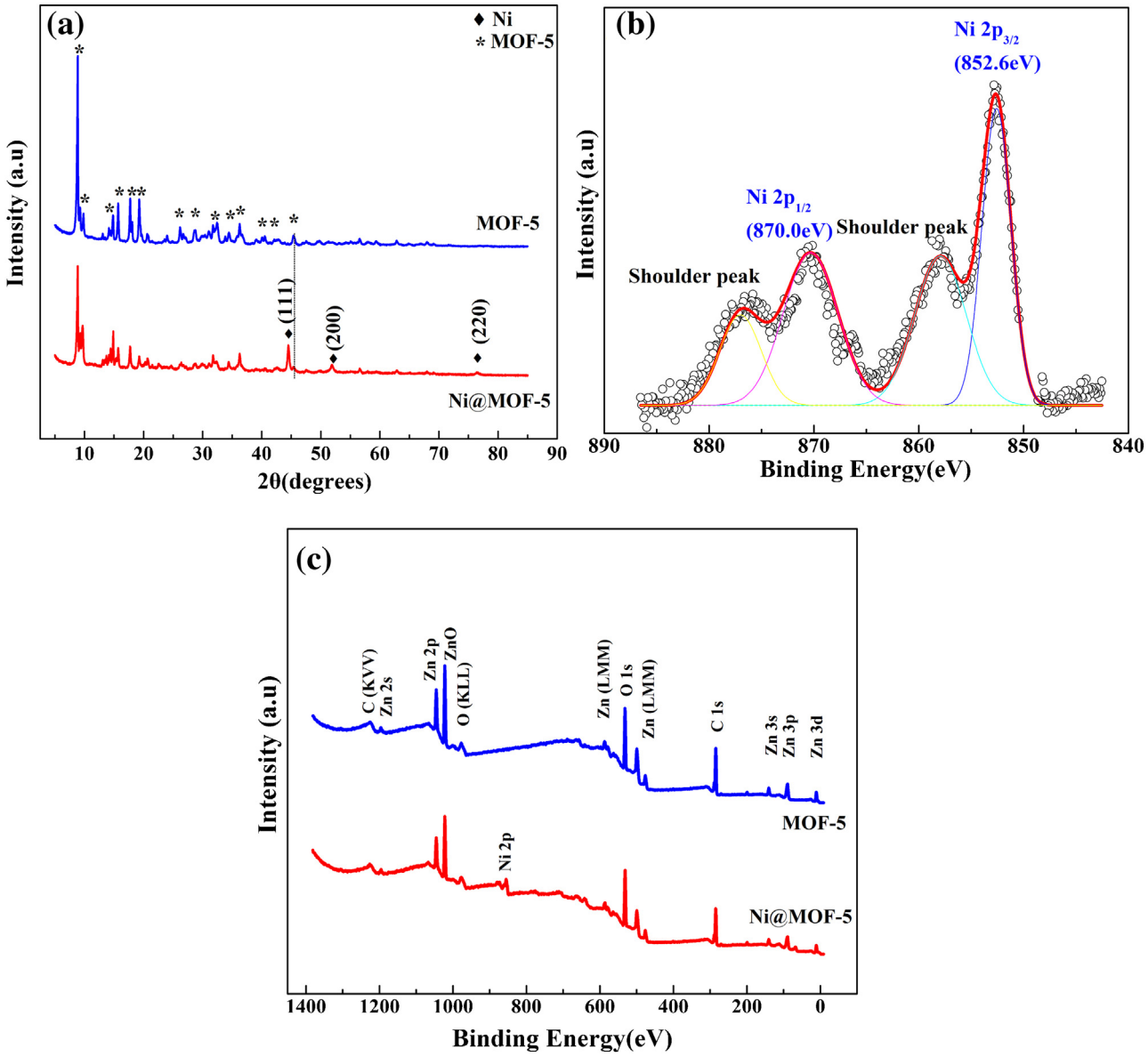

Fig. 3. (a) X-ray diffraction (XRD) patterns of MOF-5 and Ni@MOF-5 (b) Ni2p XPS spectrum for Ni@MOF-5 (c) XPS survey spectra of MOF-5 and Ni@MOF-5.

Table 1
Structural parameters obtained from N_2 adsorption isotherms analysis.

Samples	S_{BET} ($m^2\ g^{-1}$) [a]	pore volume ($cm^3\ g^{-1}$) [b]	Ni content (wt%) [c]	Ni dispersion (%) [d]
Ni@MOF-5	2961	1.037	9.73	41.8
MOF-5	2973	1.182	0	0
Ni	1.899	0.003	100	0

[a] Obtained from BET method.
[b] Total pore volume taken from the nitrogen adsorption volume at a relative pressure (P/P_0) of 0.99.
[c] The data obtained from XPS.
[d] Measured by H_2 chemisorption at 25 °C.

3.2. XRD, XPS and BET analysis

The typical XRD patterns of the MOF-5 and Ni@MOF-5 catalysts are given in Fig. 3a. The peaks at 44.5, 51.7, and 76.3° were the characteristic peaks of metallic Ni with a face-centered cubic structure (JCPDS# 87-0712). The peaks at 8.9, 9.6, 14.4, 15.7, 17.8, 19.3, 28.7, 31.8, 34.4, 36.3, and 45.5° could be assigned to the diffraction peaks of MOF-5 [54–56], which indicated that our MOF-5 support was well crystalized. The Brunauer-Emmett-Teller specific surface areas (S_{BET}) were determined by N_2 isotherms at 77 K (as shown in Table 1). The S_{BET} of Ni@MOF-5 and MOF-5 were 2961 and 2973, while that datum of metallic Ni only was 1.899 $m^2\ g^{-1}$. Meanwhile, Ni@MOF-5 had larger pore volume which would help Ni particle loading in MOF-5. Besides, according to the Ni content measured by XPS, Ni surface concentration was 9.73% over Ni@MOF-5. The Ni dispersion over MOF-5 was 41.8 measured by H_2 chemisorption, which further confirmed Ni was highly dispersed in MOF-5 support.

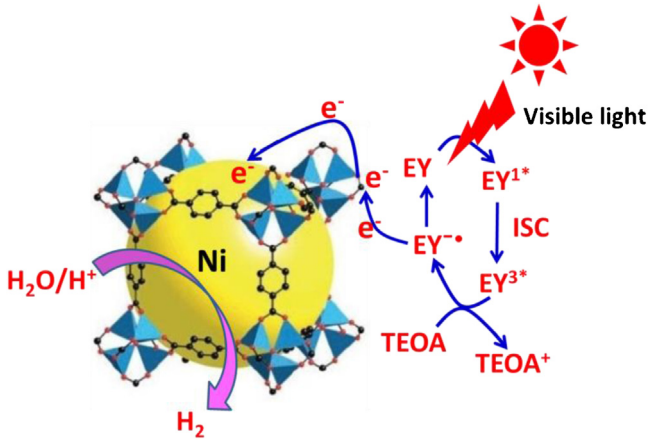

Scheme 1. Photocatalytic mechanism for H_2 evolution over the EY sensitized Ni@MOF-5 with TEOA as a Sacrificial donor under visible light irradiation.

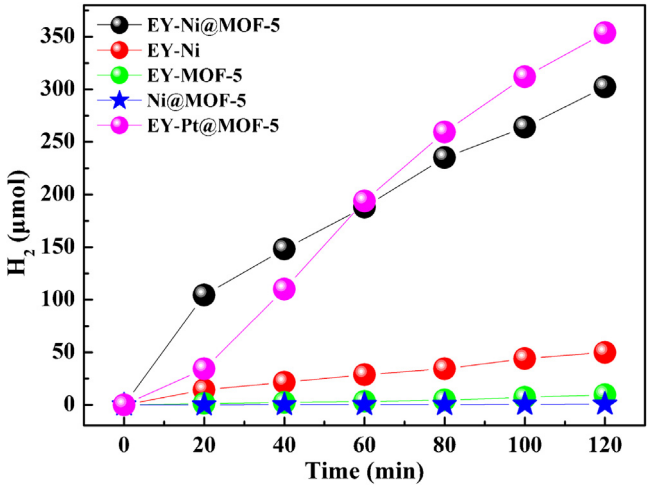

Fig. 4. The time courses of hydrogen evolution over EY-Ni, EY-MOF-5, EY-Ni@MOF-5, EY-Pt@MOF-5 and Ni@MOF-5 photocatalysts in 100 mL 10% (v/v) TEOA aqueous solution (pH 11) under visible light irradiation ($\lambda \geq 420$ nm).

The surface Ni species on Ni@MOF-5 catalysts were examined by XPS measurements and results are given in Fig. 3b. The binding energies at 852.6 and 870.0 eV could be assigned to $Ni2p_{3/2}$ and $Ni2p_{1/2}$ respectively, which indicated that Ni species was metallic state. According to the typical XPS survey (wide-scan) spectra of the Ni, MOF-5 and Ni@MOF-5 in Fig. 3c, Ni, Zn, C and O signals confirmed good crystal of used MOF-5.

3.3. The photocatalytic activities of different catalysts for H_2 evolution

The photocatalytic activities for H_2 evolution were evaluated under visible light irradiation ($\lambda \geq 420$ nm) using TEOA as sacrificial donor. Control experiments indicated that only trace amount H_2 was detected in the absence of photosensitizer EY in Ni@MOF-5, suggesting that H_2 was produced *via* sensitized photocatalytic reaction. The time courses of H_2 evolution over different catalysts showed that the anchored Ni particles in MOF-5 and the presence of EY were necessary for high efficient photocatalytic hydrogen generation (Fig. 4). In the absence of Ni nanoparticles, EY-MOF-5 only gave 9.67 μmol of H_2 after 2 h of irradiation. 49.9 μmol of H_2 was produced after 2 h of irradiation in the EY-Ni, suggesting that Ni was an active species for H_2 production. However, 302.2 μmol of H_2 evolution was evolved over the EY-Ni@MOF-5 in 2 h, which was 6.06 times higher than that of EY-Ni (49.9 μmol) with same Ni loading under the same reaction conditions. EY-Ni@MOF-5 showed little bit higher activity than EY-Pt@MOF-5 catalyst in the first 60 min. A little bit higher hydrogen evolution amount was observed over EY-Pt@MOF-5 catalyst than over EY-Ni@MOF-5 catalyst, but the rates over both catalysts were almost similar. These non-precious-metal co-catalysts (EY-Ni@MOF-5) appeared to work for efficient co-catalyst for hydrogen evolution reaction. It is known that Pt is a very good co-catalyst for hydrogen generation. That activity of EY-Ni@MOF-5 was comparable to EY-Pt@MOF-5 might due to the anchored Ni in MOFs, where MOF-5 offered a superior π-conjugated scaffold and facilitate electron transfer from dye to anchored Ni particles through MOF-5 frameworks [57,58]. High H_2 production activity might also due to the high dispersed Ni cocatalyst over large surface area (2973 m^2/g) MOF-5 (showed in Table 1).

The Ni-based catalysts with different supports (10Ni@Al_2O_3 and 10Ni@SiO_2) were also synthesized and tested for photocatalytic hydrogen generation (as shown in Fig. 5). These inorganic supports gave the retarding of the photoelectrons transfer, which finally resulted in low photocatalytic performance (as shown in Fig. 5a). Only 5.63 and 43.4 μmol of H_2 were detected in 2 h of irradiation. However, the amount of H_2 evolved was 302.2 μmol over the EY-Ni@MOF-5 photocatalyst in 2 h under same reaction conditions, which was 6.97 times higher than that of SiO_2 sample (43.4 μmol). In addition, the photocurrents of Ni@Al_2O_3 and Ni@SiO_2 were also lower than Ni@MOF-5 under the same conditions, indicating MOF-5 enhanced charge transfer (as shown in Fig. 5b).

3.4. Effect of pH and Ni NPs size on photocatalytic activity for rate of H_2 evolution over Ni@MOF-5

It was known that the solution pH had significant influence on photocatalytic activity [59]. As shown in Fig. 6, when pH values of TEOA aqueous solution varied from 5 to 13, the rate of hydrogen evolution maximized at pH 11 (30.22 mmol h^{-1} $g^{-1}_{[Ni]}$) and decreased dramatically both under more acidic and more basic reaction conditions. The decrease of rate of hydrogen evolution at acidic pH likely resulted from the protonation of TEOA, which was a less effective electron donor, thus leading to a shorter lifetime of the excited EY and lower efficiency of the excited dye species. Under strong basic condition, the thermodynamic driving force for hydrogen evolution from water decreased due to the lower concentration of H^+ [59]. Moreover, the influence of pH values on the photocatalytic activity could be partially assigned to the adsorption behavior of EY onto the frameworks of MOF-5. Min et al. reported that the adsorption of EY was mainly noncovalent and accompanied with direct interaction originated from the π-π stacking and ester-like linkage reaction between EY and carrier [57,59,60]. In the acidic solution, residual functional groups such as —COOH and —OH on the MOF-5 frameworks are protonated, so the ester like linkage forms ineffectively, while in the strong basic solution, the carboxyl groups of EY are deprotonated and the frameworks of MOF-5 is negatively charged [61,62], so the dye cannot adsorb on MOF-5 effectively because of the electrostatic repulsion force.

In a previous report, He et al. reported the loading Au nano particles on MOF-5 [51]. The diameter of the Au NP core was in the range 20 ~ 60 nm. Usually, the end size of nanoparticles is smaller than its diameter, which permits NPs loading on the locations of the open side of the pore channel of MOF-5. We loaded Ni nanoparticles in MOF-5 with different size and tested their photocatalytic activity (as shown in Fig. 7). After 2 h of irradiation, the amounts of H_2 evolution were 551.9, 380.8, and 254.6 μmol over the 3, 6, and 20 nm Ni particles photocatalyst (Ni@MOF-5), respectively. Obviously, the amount of hydrogen evolution was higher over the smaller size nickel particles. Those results might indicate that better contact of

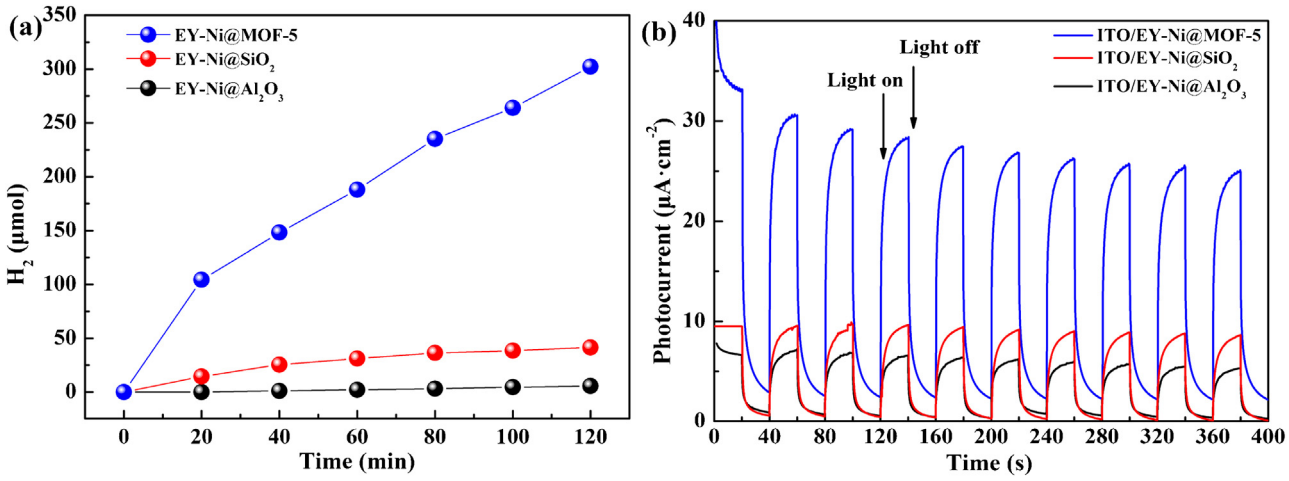

Fig. 5. The photocatalytic activity (a) and the photocurrents (b) over $Ni@Al_2O_3$, $Ni@SiO_2$ and Ni@MOF-5.

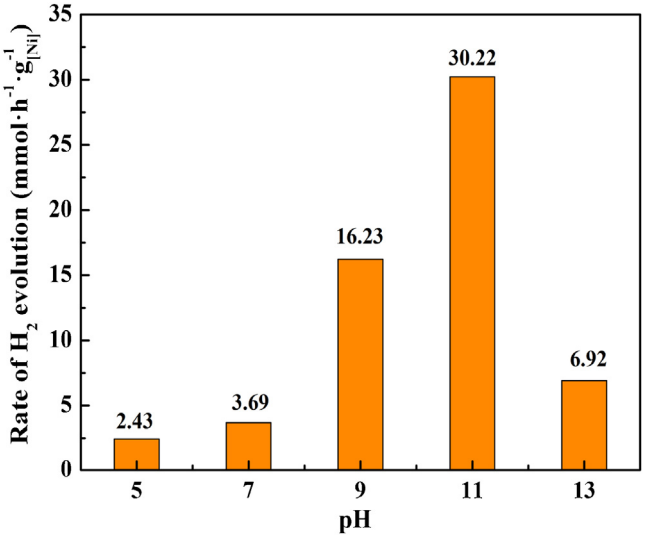

Fig. 6. Effect of pH value on photocatalytic rate of H_2 evolution over EY-Ni@MOF-5 catalyst in 100 mL 10% (v/v) TEOA aqueous solution under visible light irradiation ($\lambda \geq 420$ nm). EY: 1.0×10^{-3} mol/L.

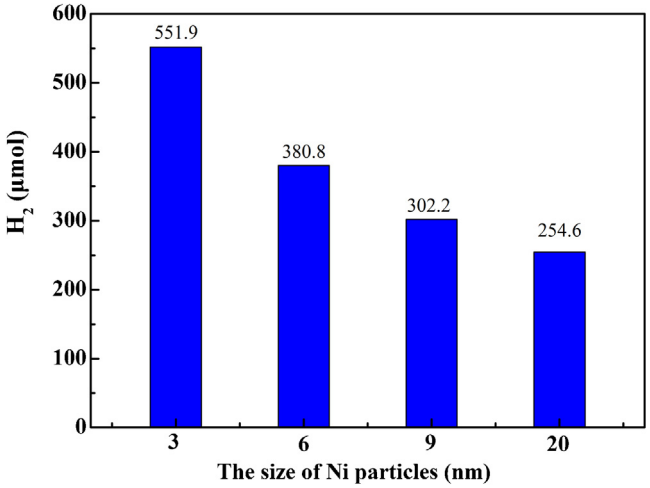

Fig. 7. Effect of Ni particles size on photocatalytic activity for amount of H_2 evolution over EY-Ni@MOF-5 catalyst in 100 mL 10% (v/v) TEOA aqueous solution under visible light irradiation ($\lambda \geq 420$ nm) 2 h. EY: 1.0×10^{-3} mol/L.

NPs with MOF-5 would lead to higher activity because of better contact of Ni particles with MOF-5 for smaller size of Ni NPs.

3.5. Fluorescence lifetime and transient photocurrent-time test

To prove the role of MOF-5 in facilitating the transfer of photogenerated electrons, the photoluminescence quenching of EY in the presence of the Ni, MOF-5, Pt@MOF-5 and Ni@MOF-5 were examined (shown in Fig. 8A). The aqueous EY solution showed an intensive emission peak centered at 527 nm, which was caused by its strong recombination of excited charge pairs by exciting light [59,61]. When Ni, MOF-5, Ni@MOF-5 and Pt@MOF-5 were introduced, there was a significant decrease in the peak intensity of EY emission, meanwhile, slight red shifts (~8 nm) of the emission peak were observed. Thus shifts could be mainly ascribed to the noncovalent $\pi-\pi$ interaction of MOF-5 with EY and the interfacial electron transfer from the attached EY^* to the MOF-5 frameworks, and to Ni surface. Tanaka et al. and Zhang et al. reported MOFs with π-conjugated organic linkers could promote the charge transfer [63,64]. Zhang et al. found that electron formed in dye molecule could transfer from the dye to the catalyst surface when dye adsorbed by offset face-to-face orientation *via* π-π conjugation between MB and aromatic regions of the graphene [60]. Then it is reasonable to assume that the electron transfers from excited dye to MOF-5 through the π-π interactions, and finally electron transfers to Ni surface.

To further prove a strong interaction between EY and MOF-5, the adsorption amount of EY on nano-Ni and MOF-5 was checked by static adsorption method (as shown in Fig. 9). It is clear that MOF-5 has the larger adsorption amount of EY, the corresponding adsorption amount of EY is 10.5 mg/g over the MOF-5 by static adsorption in 24 h, which is 4.2 times higher than that of the same weight of Nano-Ni (2.6 mg/g) under the same adsorption conditions (the concentration of EY was 12 mg/L). It confirms that there is a strong interaction between EY and MOF-5. In fact, the fluorescence intensity of EY-Ni@MOF-5 was the weakest among all the tested samples.

The fluorescence lifetimes of EY in the presence of Ni, MOF-5, Ni@MOF-5 and Pt@MOF-5 were investigated to probe the excited charge transfer. The fluorescence lifetimes were obtained by fitting the decay profiles with one exponential term and two exponential terms, respectively. In Table 2, the emission of singlet excited EY gave a lifetime of 1.18 ns, which increased slightly in the presence of Ni (1.21 ns) or MOF-5(1.22 ns). In contrast, we observed an enhanced decay of the singlet excited state of EY with the addition

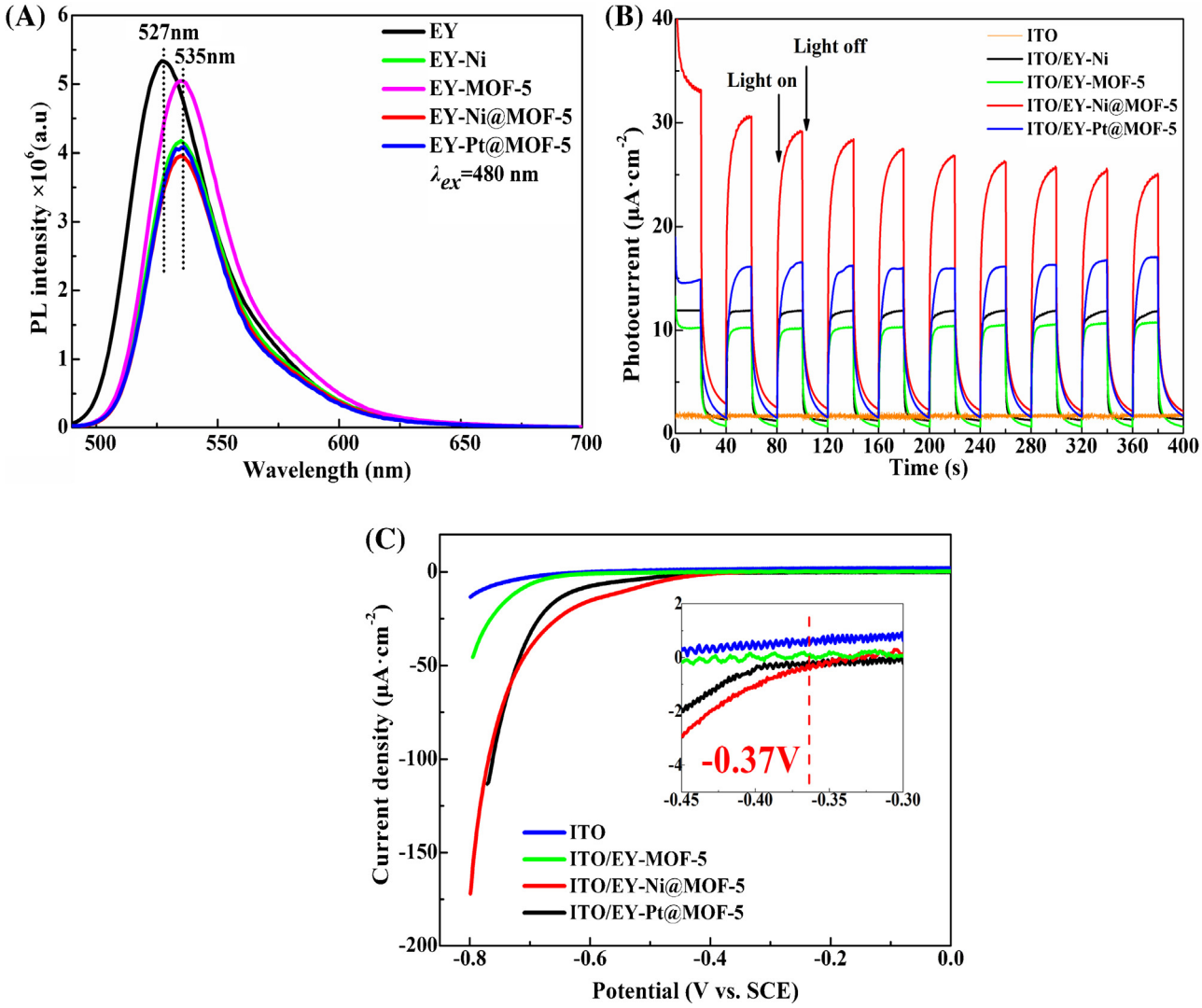

Fig. 8. (A) Photoluminescence quenching (excitation wavelength of 480 nm) of EY (1.0×10^{-6} mol/L) by Ni, MOF-5, Ni@MOF-5 and Pt@MOF-5 in 10% (v/v) TEOA aqueous solution at pH 11. [Catalysts]: 0.5 mg/mL. (B) Transient photocurrent–time profiles of EY-sensitized Ni, MOF-5, Ni@MOF-5 and Pt@MOF-5 coated on ITO glass in a mixed solution of 10% (v/v) TEOA and Na_2SO_4 (0.1 mol/L) at pH 11 under visible light irradiation ($\lambda \geq 420$ nm). (C) LSV curves of bare ITO glass and MOF-5, Ni@MOF-5 and Pt@MOF-5 coated on ITO electrodes in a mixed solution of 10% (v/v) TEOA and 0.1 mol/L Na_2SO_4 at pH 11. The scan rate was 1 mV s^{-1}.

Table 2
Decay parameters of EY in the presence of Ni, MOF-5 and Ni@MOF-5 in 10% (v/v) TEOA aqueous solution at pH 11.

Systems [a]	Lifetime,<τ> (ns)	Pre-exponential factors *A*	Average lifetime,<τ> (ns) [d]	χ^2
EY [b]	1.18	A = 0.370	1.18	1.003
EY-Ni [c]	τ_1 = 1.00	A_1 = 0.060	1.21	1.000
	τ_2 = 1.64	A_2 = 0.018		
EY-MOF-5 [c]	τ_1 = 0.01	A_1 = 0.053	1.22	1.003
	τ_2 = 1.25	A_2 = 0.024		
EY-Ni@MOF-5 [c]	τ_1 = 0.91	A_1 = 0.050	1.26	0.999
	τ_2 = 1.48	A_2 = 0.029		
EY-Pt@MOF-5 [c]	τ_1 = 0.95	A_1 = 0.027	1.25	1.007
	τ_2 = 1.69	A_2 = 0.010		

[a] Decay of TEOA aqueous solution (10% v/v) of 1.0×10^6 mol/L EY at pH 11 was recorded in the presence of 0.5 mg/L Ni, MOF-5 and Ni@MOF-5. The excited and emission wavelength were 480 nm and 528 nm, respectively.
[b] Single-exponential fit for EY.
[c] Double-exponential fit for EY-Ni, EY-MOF-5, EY-Ni@MOF-5 and EY-Pt@MOF-5.
[d] Average lifetime <τ> was determined according to reported method [66].

of the Ni@MOF-5 (1.26 ns), and this decay trace deviated from the single exponential behavior. The fitted results with two exponential decay functions indicated the presence of dynamic quenching. The lifetimes of short and long decay components were 0.91 and 1.48 ns respectively, which could be attributed to the excited state of EY in the MOF-5-bound and the unbound states [57]. Lazarides et al. also reported that no quenching of the singlet fluorescence of dyes EY when either TEOA or catalyst was added; indicating that the singlet excited state did not take part in electron transfer [65]. The initially formed singlet excited state (EY^{1*}) changed to its lowest-lying

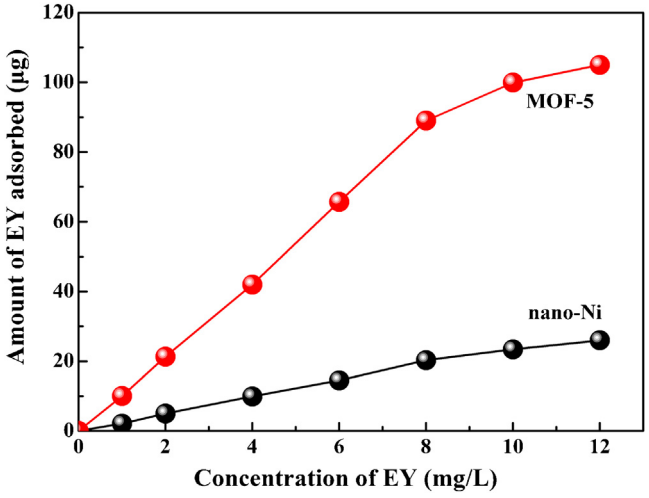

Fig. 9. Effect of the Nano-Ni and MOF-5 on the adsorption Eosin Y [MOF-5 or Nano-Ni was 10 mg; EY: 10 mL] by static adsorption method.

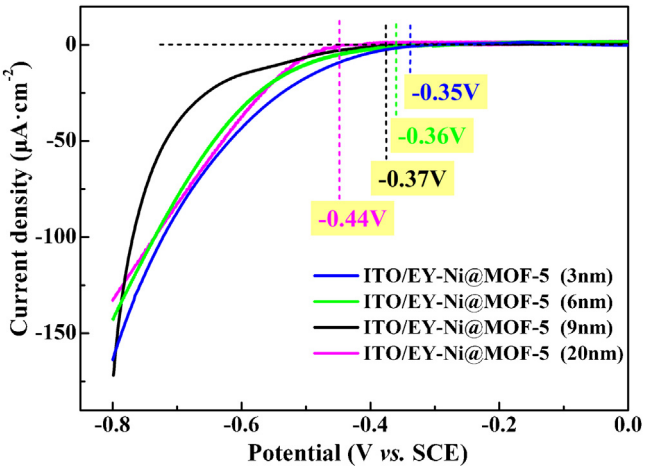

Fig. 10. LSV curves of different Ni particles size (ITO/EY-Ni@MOF-5) electrodes in a mixed solution of 10% (v/v) TEOA and 0.1 mol/L Na_2SO_4 at pH 11. The scan rate was 1 mV s^{-1}.

triplet excited state (EY^{3*}) intermediates *via* intersystem crossing (ISC).

Above results indicated that MOF-5 could greatly prolong the lifetime of the singlet excited EY^* in the Ni@MOF-5 systems, which could greatly facilitate the intersystem crossing (ISC) to produce the low-lying triplet excited state (EY^{3*}) and then to form $EY^{-\bullet}$ in the presence of TEOA. Due to the excellent electron capturing ability of MOF-5, electrons are then transferred from $EY^{-\bullet}$ to MOF-5 and then to Ni, where the protons are reduced to form molecular H_2. By comparing the fluorescence lifetime of EY-Ni@MOF-5 (1.26 ns) with EY-Pt@MOF-5 (1.25 ns), EY-Ni@MOF-5 showed the largest fluorescence lifetime, which corresponded its higher photocatalytic hydrogen evolution activity.

To provide additional evidence for the above suggested electron transfer mechanism, the transient photocurrent responses of EY sensitized Ni, MOF-5, Ni@MOF-5 and Pt@MOF-5 electrodes coated on ITO were recorded for several on-off cycles under visible light irradiation (Fig. 8B). It is apparent that the ITO/EY-Ni@MOF-5 electrode exhibits a noticeable higher photocurrent, which indicates the improvement of the electron transfer from excited dye to Ni@MOF-5. In addition, the transient photocurrent response of EY sensitized Pt@MOF-5 electrode coated on ITO is weaker than Ni@MOF-5 electrode. These results indicate the fast interfacial electron transfer from $EY^{-\bullet}$ to Ni@MOF-5. The oxidative dye species will be captured or reductively quenched by the TEOA on the photoelectrode surface. That is, MOF-5 can promote the charge transfer in the EY-Ni@MOF-5 and thus lower the charge recombination possibilities. Therefore, MOF-5 can serve as a good electron acceptor and transporter, and suppress the recombination processes of photogenerated charges effectively and thus enhance the photocatalytic H_2 evolution activity under visible light.

The electrochemical H_2 generation activities of ITO/EY-MOF-5, ITO/EY-Ni@MOF-5 and ITO/EY-Pt@MOF-5 electrodes were also investigated by the linear sweep voltammetry (LSV) technique (shown in Fig. 8C). The cathodic current related to the reduction of water to H_2 on bare ITO electrode was extremely low even at high applied potentials. But ITO/EY-MOF-5 showed an increased cathodic current at a similar potential range, clearly indicating that the MOF-5 material was a good electrocatalyst that could efficiently catalyze the reduction of water to H_2 [57]. Loading Ni and Pt led to significant decrease of over-potential for hydrogen evolution. The comparison results of 9 nm Ni and Pt in MOF-5 are given in Fig. 5 Fig. 8C. The over-potential EY-Ni@MOF-5 electrode of hydrogen generation was −0.37 V, which was similar to the datum of EY-Pt@MOF-5 electrode. We also compared the EY-Ni@MOF-5 electrodes with different Ni particle diameter, and the results indicated that smaller particle led to the lower over-potential. 20 nm Ni particles present −0.44 V over-potential, while 9 nm Ni particles gave the −0.37 V over-potential (as shown in Fig. 10). Further decrease of Ni particle diameter led to even lower over-potential, 6 nm and 3 nm Ni particles gave −0.36 and −0.35 V over-potentials respectively. It seems that the decrease tendency of over-potential becomes weak when the Ni particle diameter decreases from 6 nm to 3 nm; however, −0.37 V is a quite low over-potential. Since the photocatalytic activity of hydrogen evolution is highly dependent on the over-potential HER reaction [67], smaller Ni particles offered the catalyst a better activity for hydrogen evolution.

3.6. Electrochemical impedance spectroscopy analysis of Ni@MOF-5 samples with different exposed facets

It is known that the electrochemical HER over metal NPs is structure sensitive reaction. For example, Cui et al. disclosed that the exposed facets of metal-NPs showed significant effects on photocatalytic properties [68]. To further demonstrate the electron transfer from MOF-5 to Ni surface with different crystal facets, we synthesized Ni@MOF-5 samples with different exposed facets ((1 1 1), (1 1 1/2 0 0), and (2 0 0)) of Ni. Fig. 11 gives the typical TEM and HRTEM images of Ni NPs and Ni@MOF-5 samples as-prepared. As shown in Fig. 11a, a cubic shape was obtained which suggested the existence of (1 0 0) surface structure. The same results were also confirmed by HRTEM characterization (Fig. 11a-2). The lattice spacing parallel to the top and bottom facets was 0.176 nm, corresponding to the (2 0 0) planes of Ni. The Ni NPs shape was predominantly hexagonal (as shown in Fig. 11b), suggesting the coexistence of (2 0 0) and (1 1 1) Ni surface domains. The lattice spacing of 0.204 nm observed in HRTEM image (Fig. 11b-2) correspondeds to the (1 1 1) planes of Ni, which proved that there were (1 1 1) existing in hexagonal Ni. The Ni NPs with tetrahedral shapes were observed (Fig. 11c). The *d*-spacing of adjacent fringe for Ni nanocrystals was 0.204 nm, that could be indexed to the (1 1 1) crystalline plane of Ni (shown in Fig. 11c-2). Additionally, the images showed that the Ni NPs were in good dispersion in the frameworks of MOF-5(Fig. 11a-1, b-1, and c-1). Selected area electron diffraction (SAED) was also used to comfirm the cubic structure of the Ni (2 0 0) NPs. (Fig. 11a-3). Likewise, SAED of Ni(2 0 0/1 1 1) and Ni(1 1 1) NPs also be given to comfirm the predominantly hexagonal and tetrahedral shapes Ni particles.

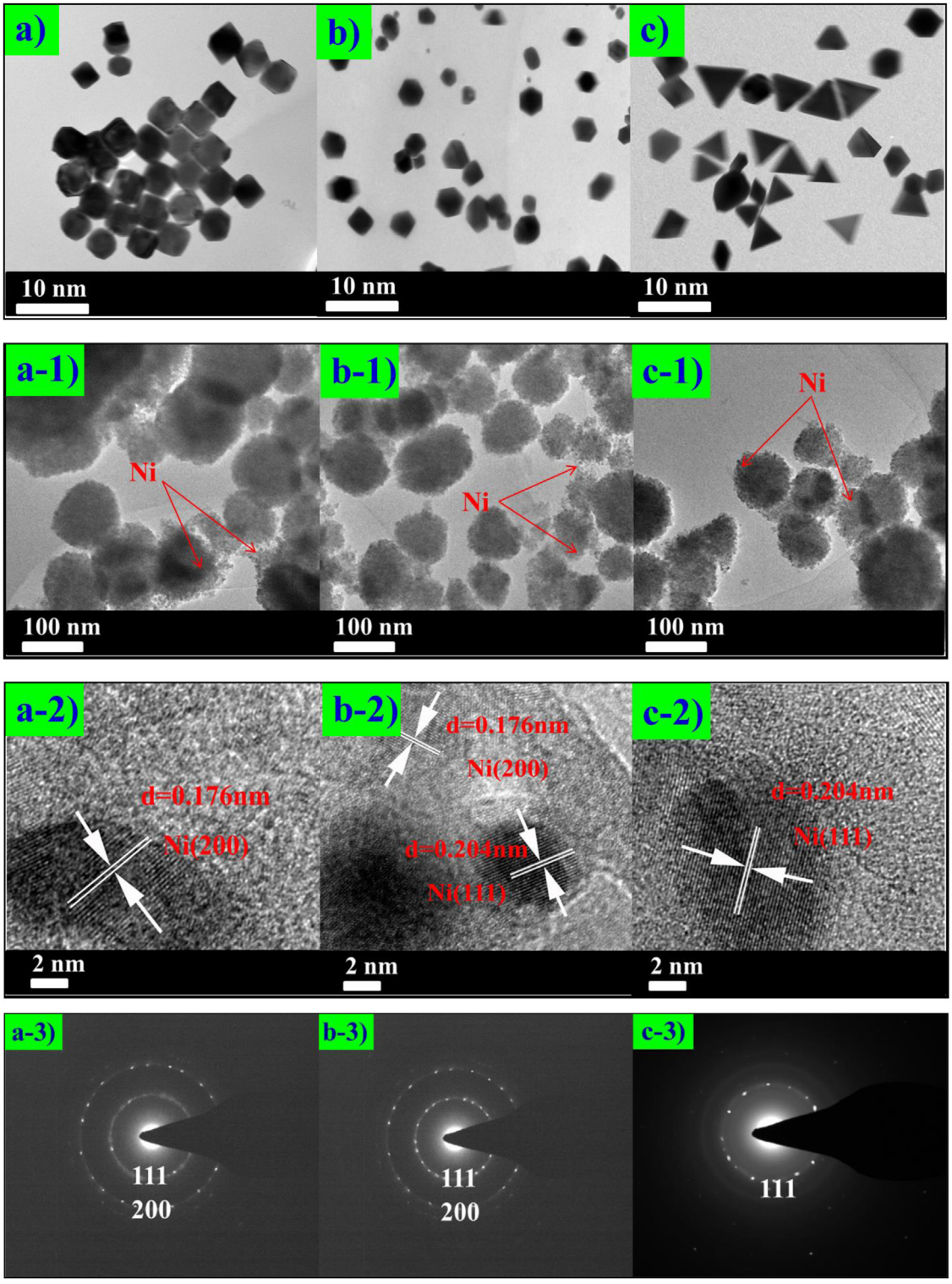

Fig. 11. TEM images of Ni(2 0 0)(a), Ni(2 0 0/1 1 1)(b), and Ni(1 1 1)(c) nanoparticles, respectively; TEM and HRTEM images of Ni(2 0 0)(a), Ni(2 0 0/1 1 1)(b), and Ni(1 1 1)(c) NPs, respectively; TEM and HRTEM images of Ni(2 0 0)@MOF-5(a-1;a-2), Ni(2 0 0/1 1 1)@MOF-5(b-1;b-2), and Ni(1 1 1)@MOF-5(c-1;c-2) samples, respectively. SAED pattern of (a-3) Ni(2 0 0), (b-3) Ni(2 0 0/1 1 1) and (c-3) Ni(1 1 1) NPs.

Fig. 12 displays the Nyquist plots of electrochemical impedance spectroscopy (EIS). In Nyquist plots, the Ni(1 1 1)@MOF-5 sample showed the smallest semicircle in the middle-frequency region compared with those of Ni(2 0 0)@MOF-5 and Ni(1 1 1/2 0 0)@MOF-5 electrodes under light irradiation, indicating the introduction of Ni(1 1 1) NPs promoted the electrons transfer from the MOF-5.

3.7. Hydrogen source analysis

In order to identify hydrogen generated *via* water splitting, the isotopic tracer experiments were carried out (as shown in Fig. 13). Since Triethanolamine-D15 was hard to purchase, we used CD_3OD and D_2O as reactants. The gas products were analysed by Gas Chromatography Mass Spectrometer (GC–MS). In

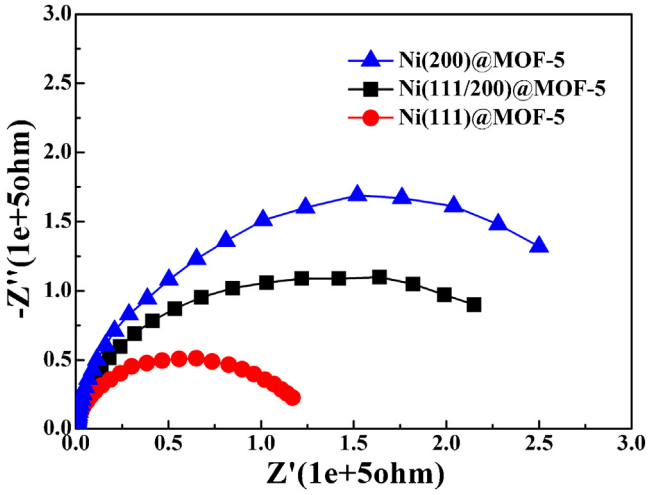

Fig. 12. EIS Nyquist plots of Ni@MOF-5 film electrodes under light irradiation. The curves was Ni(2 0 0)@MOF-5, Ni(1 1 1/2 0 0)@MOF-5, and Ni(1 1 1)@MOF-5 samples, respectively.

the mixture of CH_3OH + TEOA + EY-Ni@MOF-5 without water, no hydrogen was detected under illumination (experiment a). But both D_2 and H_2 were detected when D_2O was added (in the mixture of CH_3OH + TEOA + D_2O + EY-Ni@MOF-5, experiment b). Only H_2 was detected in the mixture of CD_3OD + H_2O + EY-Ni@MOF-5 (experiment c). Experiment b gave higher D_2 while experiment c only gave H_2. Trace amount of H_2 formation in experiment b might due to the proton exchange of D_2O and CH_3OH. In the CD_3OD and H_2O experiment, only H_2 was detected without D_2. This indicated that the H_2 was from H_2O rather than from sacrificing reagents (as shown in Fig. 13c). Previous papers present similar results [60–70].

3.8. Apparent quantum efficiencies and stability tests

To investigate the wavelength dependence of photocatalytic H_2 evolution, the apparent quantum efficiencies (AQEs) of EY-Ni@MOF-5 for hydrogen evolution were examined over a wide visible light range of 430–550 nm. As shown in Fig. 14A, it can be seen that the AQEs decreases with increasing wavelengths. The highest AQE of the EY-Ni@MOF-5 system was 16.7% at 430 nm. However, another high AQE was obtained at 520 nm, which corresponded to the highest absorption wavelength of EY (518 nm) (Fig. 15). These results indicated that the hydrogen evolution reaction was indeed driven by the input light adsorbed by EY [59].

The stability tests of EY-Ni@MOF-5 and EY-Pt@MOF-5 were checked, and the results were shown in Fig. 14B. It was found that in the first run, the maximum amounts of photocatalytic H_2 evolution were 302.2 μmol and 353.7 μmol, respectively. Ni@MOF-5

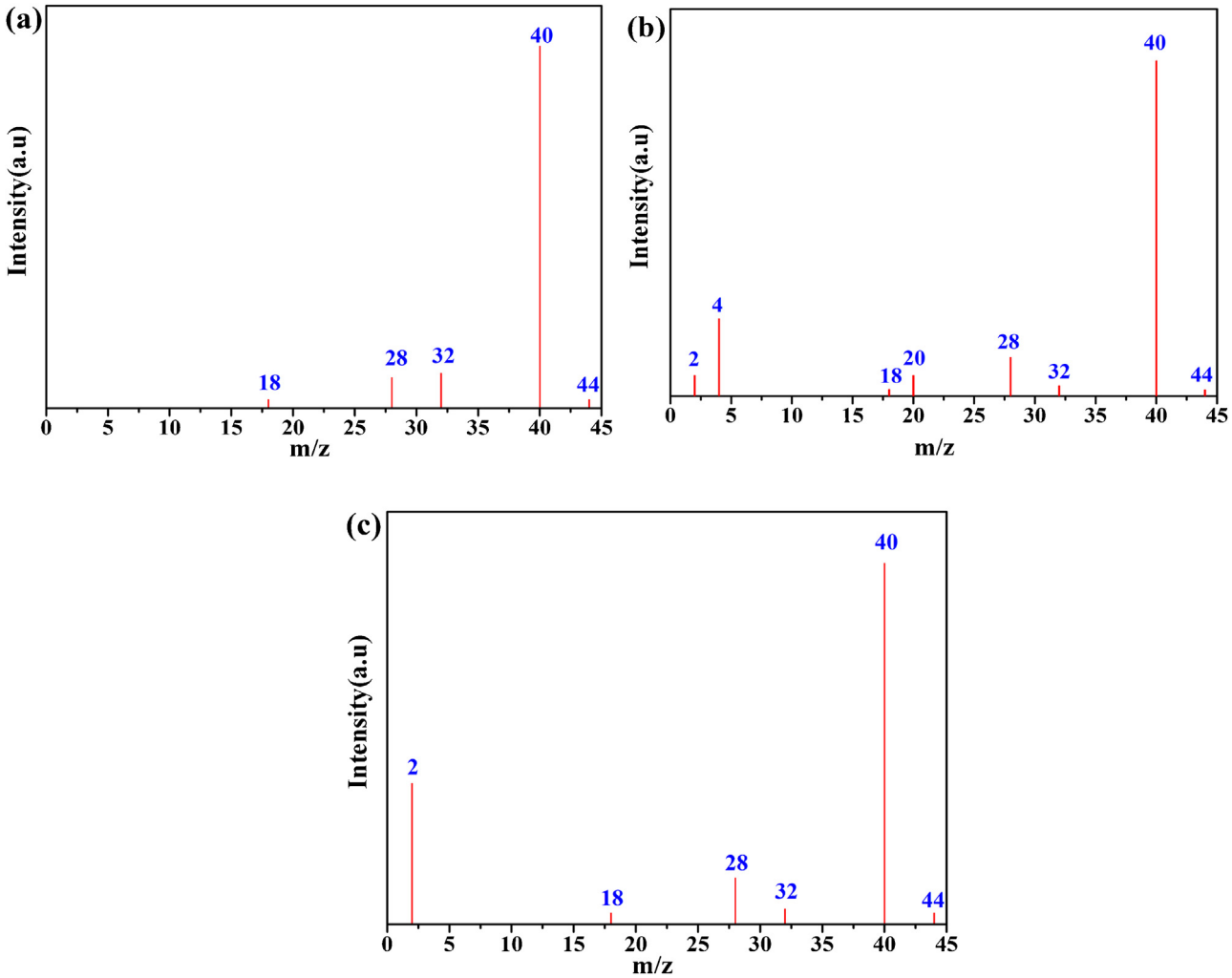

Fig. 13. GC–MS spectra obtained after injecting 0.5 mL samples of the gas phase species produced during illumination 24 h [(a) CH_3OH + TEOA + EY-Ni@MOF-5, CH_3OH:TEOA = 1:1 (v/v); (b) CH_3OH + TEOA + D_2O + EY-Ni@MOF-5, CH_3OH:TEOA:D_2O = 0.5:0.5:9; (c) CD_3OD + H_2O + EY- Ni@MOF-5, CD_3OD: H_2O = 1:9].

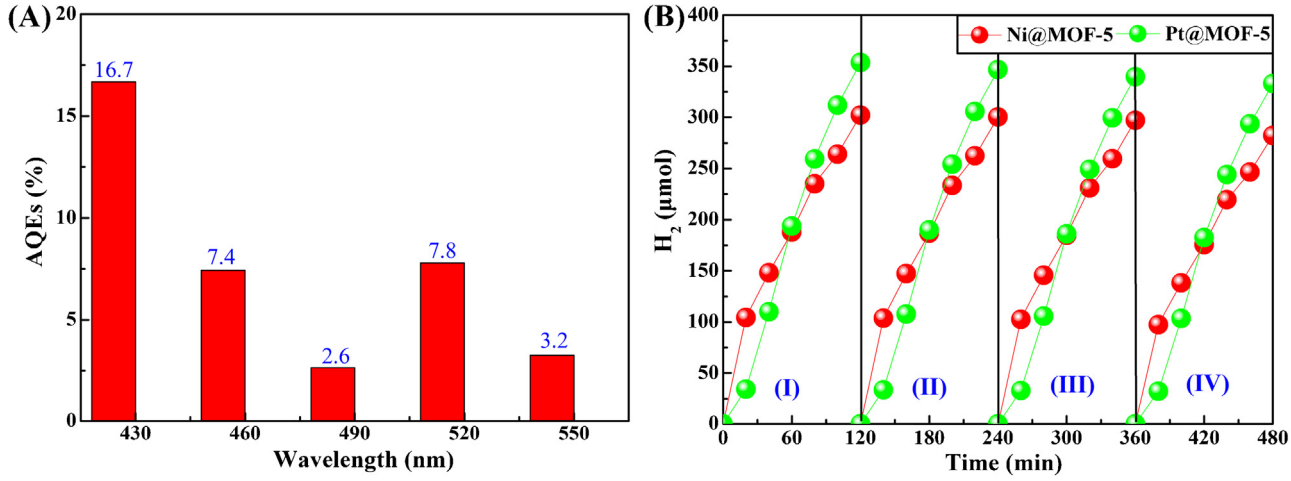

Fig. 14. (A) Apparent quantum efficiencies (AQEs) of H_2 evolution for EY (1.0×10^{-3} mol/L) photosensitized systems catalyzed by Ni@MOF-5 in 100 mL 10% (v/v) TEOA aqueous solution (pH 11) under light irradiation with different wavelengths. The system was irradiated by a 300-W Xe lamp with a cutoff filter of 420 nm and a band pass filter. Irradiation time: 30 min. (B) Stability test and comparison of H_2 evolution over EY sensitized Ni@MOF-5 and Pt@MOF-5 in 100 mL 10% (v/v) TEOA aqueous solution (pH 11) under visible light irradiation (λ ≥420 nm). The reaction was continued for 480 min, with evacuation every 120 min. (I) First run (II) add EY and TEOA, and evacuation (III) repeat II (IV) repeat III. The system was irradiated by a 300-W Xe lamp with an optical cut-off filter of 420 nm.

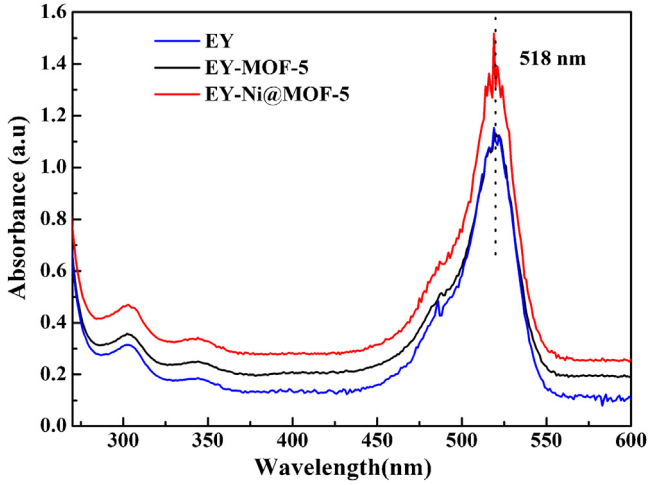

Fig. 15. UV–vis absorption spectra of EY and EY (1×10^{-5} M) sensitized MOF-5, Ni@MOF-5 in 10% (v/v) TEOA aqueous solution at pH 11.

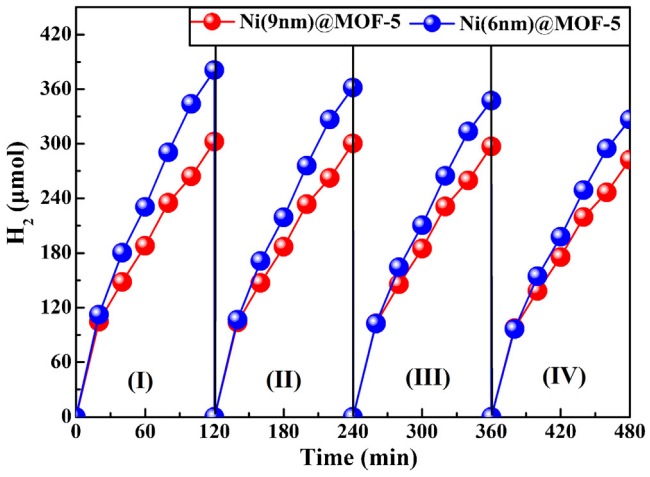

Fig. 16. Stability test and comparison of H_2 evolution over EY sensitized Ni(6 nm)@MOF-5 and Ni(9 nm)@MOF-5 in 100 mL 10% (v/v) TEOA aqueous solution (pH 11) under visible light irradiation (λ ≥420 nm). The reaction was continued for 480 min, with evacuation every 120 min. (I) First run (II) add EY and TEOA, and evacuation (III) repeat II (IV) repeat III. The system was irradiated by a 300-W Xe lamp with an optical cutoff filter of 420 nm.

and Pt@MOF-5 showed similar photocatalytic activities and stabilities. For Ni@MOF-5, the H_2 evolution activity of Ni@MOF-5 could be revived to 99% by the concurrent addition of EY and TEOA (v/v = 10%, pH 11) under visible light irradiation (λ ≥ 420 nm) in the second run. Hence, Ni@MOF-5 was relatively stable during the photocatalytic H_2 evolution. We also compared the stabilities of Ni(6 nm)@MOF-5 and Ni(9 nm)@MOF (Fig. 16). The slight decrease of activity over Ni(6 nm)@MOF-5 was observed. It implied that Ni(9 nm)@MOF-5 was comparatively stable during the photocatalytic H_2 evolution processes.

3.9. The analysis of used catalyst Ni@MOF-5 with XRD, XPS after stability test

In order to study the structural of used catalyst, we have characterized the Ni@MOF-5 (used) catalyst with XRD, and XPS techniques. In Fig. 17a, the similar intensities of peaks at 44.5, 51.7, and 76.3° over Ni@MOF-5 belonged to the (1 1 1) (2 0 0) and (2 2 0) planes of metallic Ni with a face-centered cubic structure (JCPDS# 87-0712), which implied that the fresh and used catalyst had no significant difference on the distribution of Ni species. In Fig. 17b, the binding energies at 852.6 and 870.0 eV could be assigned to $Ni2p_{3/2}$ and $Ni2p_{1/2}$, respectively. It indicated that Ni species was metallic Ni over Ni@MOF-5. These results further suggested that the Ni@MOF-5 photocatalyst performed the excellent stability during the long-term tests.

3.10. Photocatalytic Mechanism for H_2 Evolution over Ni@MOF-5

The high H_2 evolution activity of the Ni@MOF-5 catalyst in a dye-sensitized system can be depicted in Scheme 1. MOF-5 have extremely large surface area of ~2900 m^2 g^{-1}, well-ordered porous structures and channels, and is conducive to the electron transfer. Under visible light irradiation, the Eosin Y absorbs light photon to form singlet excited state EY^{1*}, which subsequently produces a lowest-lying triplet excited state EY^{3*} *via* an efficient intersystem crossing (ISC). In the presence of TEOA as a sacrificial donor, EY^{3*} can be reductively quenched and produce $EY^{-\bullet}$ [37,65,71]. These $EY^{-\bullet}$ species preferentially transfer their electrons to *via* MOF-5

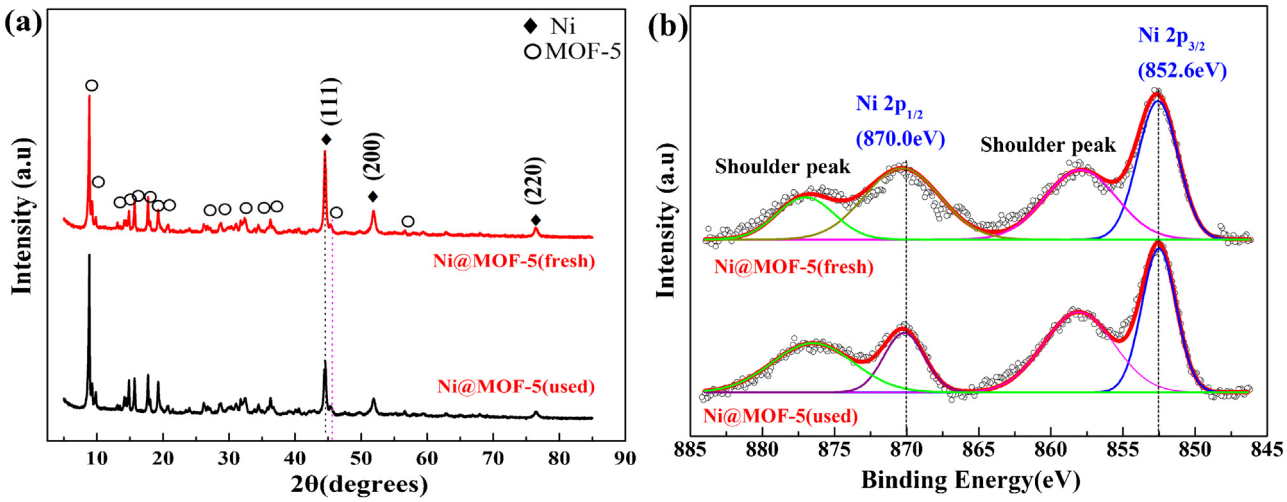

Fig. 17. (a) XRD pattern and (b) Ni2p XPS spectrum of Ni@MOF-5 (fresh and used).

frameworks due to its electron transport characteristics. The accumulated electrons on the MOF-5 frameworks will transfer to the Ni species, and finally H^+ obtains electrons from Ni to form hydrogen. MOF-5 can function as an excellent electron acceptor and transporter to efficiently prolong the lifetime of charge carriers and consequently improve the charge separation efficiency and the catalytic H_2 evolution activity of the Ni@MOF-5.

4. Conclusions

In summary, we prepared high active co-catalyst for H_2 evolution, Ni anchored on the frameworks of MOF-5, by impregnation and *in situ* chemical reduction methods. The Ni@MOF-5 possessed high specific surface area (2961 m^2/g), high dispersion (41.8%), and small-sized nickel particles (~9 nm) resulted in the low over-potential of −0.37 V, which have the similar over-potential as Pt@MOF-5, and exhibited the excellent photocatalytic activity and stability for hydrogen evolution. The Ni@MOF-5 material had the larger transient photocurrent and longer fluorescence lifetime. Moreover, Ni NPs with exposed (1 1 1) facets was more benefited the electrons transfer from MOF-5 to Ni than that of (2 0 0) facets. MOF-5 might promote the photogenerated electrons transfer from excited EY to the hydrogen evolution active sites (Ni), and consequently enhance photocatalytic hydrogen evolution efficiency. The rate of H_2 evolution reached 30.22 mmol h^{-1} $g^{-1}_{[Ni]}$ over the EY-sensitized Ni@MOF-5 irradiated under visible light irradiation ($\lambda \geq 420$ nm) in 2 h. The apparent quantum efficiency (AQE) of 16.7% over EY-Ni@MOF-5 was achieved under 430 nm illuminations.

Acknowledgements

This work has been supported by the 973 Program of Department of Sciences and Technology China (Grant No. 2013CB632404) and by the National Natural Science Foundation of China (Grant No.21433007 and 21373245).

References

[1] M.S. Dresselhaus, I.L. Thomas, Nature 414 (2001) 332–337.
[2] Z. Li, C. Kong, G. Lu, J. Phys. Chem. C 119 (2015) 13561–13568.
[3] S. Peng, M. Ding, T. Yi, Y. Li, J. Mol. Catal. (China) 28 (2014) 466–473.
[4] C. Wang, J. Wang, W. Lin, J. Am. Chem. Soc. 134 (2012) 19895–19908.
[5] A.L. Linsebigler, G. Lu, J.T. Yates, Chem. Rev. 95 (1995) 735–758.
[6] M. Matsuoka, M. Kitano, M. Takeuchi, K. Tsujimaru, M. Anpo, J.M. Thomas, Catal. Today 122 (2007) 51–61.
[7] Y. Di, X.C. Wang, A. Thomas, M. Antonietti, ChemCatChem 2 (2010) 834–838.
[8] Y. Li, H. Wang, L. Xie, Y. Liang, G. Hong, H. Dai, J. Am. Chem. Soc. 133 (2011) 7296–7299.
[9] W. Zhen, B. Li, G. Lu, J. Ma, RSC Adv. 4 (2014) 16472–16479.
[10] A. Baylet, S. Royer, P. Marécot, J.M. Tatibouët, D. Duprez, Appl. Catal. B: Environ. 81 (2008) 88–96.
[11] J. Dawody, M. Skoglundh, S. Wall, E. Fridell, J. Mol. Catal. A: Chem. 225 (2005) 259–269.
[12] Y. Nagai, T. Hirabayashi, K. Dohmae, N. Takagi, T. Minami, H. Shinjoh, S. Matsumoto, J. Catal. 242 (2006) 103–109.
[13] Y. Li, R. Yang, Langmuir 23 (2007) 12937–12944.
[14] Y.L. Liu, V.C. Kravtsov, R. Larsen, M. Eddaoudi, Chem. Commun. (2006) 1488–1490.
[15] U. Mueller, M. Schubert, F. Teich, H. Puetter, K. Schierle-Arndt, J. Pastré, J. Mater. Chem. 16 (2006) 626–636.
[16] J. He, Z. Yan, J. Wang, J. Xie, L. Jiang, Y. Shi, F. Yuan, F. Yu, Y. Sun, Chem. Commun. 49 (2013) 6761–6763.
[17] M. Eddaoudi, J. Kim, N. Rosi, D. Vodak, J. Wachter, M. O'Keeffe, O.M. Yaghi, Science 295 (2002) 469–472.
[18] L.J. Murray, M. Dincă, J.R. Long, Chem. Soc. Rev. 38 (2009) 1294–1314.
[19] A.R. Millward, O.M. Yaghi, J. Am. Chem. Soc. 127 (2005) 17998–17999.
[20] J. Kim, S.T. Yang, S.B. Choi, J. Sim, J. Kim, W.S. Ahn, J. Mater. Chem. 21 (2011) 3070–3076.
[21] P. Horcajada, T. Chalati, C. Serre, B. Gillet, C. Sebrie, T. Baati, J.F. Eubank, D. Heurtaux, P. Clayette, C. Kreuz, J.S. Chang, Y.K. Hwang, V. Marsaud, P.N. Bories, L. Cynober, S. Gil, G. Férey, P. Couvreur, R. Gref, Nat. Mater. 9 (2010) 172–178.
[22] P. Horcajada, C. Serre, G. Maurin, N.A. Ramsahye, F. Balas, M. Vallet-Regí, M. Sebban, F. Taulelle, G. Férey, J. Am. Chem. Soc. 130 (2008) 6774–6780.
[23] J. Kim, S. Bhattacharjee, K.E. Jeong, S.Y. Jeong, W.S. Ahn, Chem. Commun. (2009) 3904–3906.
[24] D. Farrusseng, S. Aguado, C. Pinel, Angew. Chem. Int. Ed. 48 (2009) 7502–7513.
[25] L. Alaerts, E. Séguin, H. Poelman, F. Thibault-Starzyk, P.A. Jacobs, D.E. De Vos, Chem. Eur. J. 12 (2006) 7353–7363.
[26] M. Alvaro, E. Carbonell, B. Ferrer, F.X. Llabrés i Xamena, H. Garcia, Chem. Eur. J. 13 (2007) 5106–5112.
[27] C. Wang, D. Liu, W. Lin, J. Am. Chem. Soc. 135 (2013) 13222–13234.
[28] D. Sun, Y. Fu, W. Liu, L. Ye, D. Wang, L. Yang, X. Fu, Z. Li, Chem. Eur. J. 19 (2013) 14279–14285.
[29] H. Wang, X. Yuan, Y. Wu, G. Zeng, X. Chen, L. Leng, H. Li, Appl. Catal. B: Environ. 174 (2015) 445–454.
[30] H. Wang, X. Yuan, Y. Wu, X. Chen, L. Leng, G. Zeng, RSC Adv. 5 (2015) 32531–32535.
[31] D. Sun, L. Ye, Z. Li, Appl. Catal. B: Environ. 164 (2015) 428–432.
[32] Y. Fu, D. Sun, Y. Chen, R. Huang, Z. Ding, X. Fu, Z. Li, Angew. Chem. Int. Ed. 51 (2012) 3364–3367.
[33] D. Wang, R. Huang, W. Liu, D. Sun, Z. Li, ACS Catal. 4 (2014) 4254–4260.
[34] Y. Horiuchi, T. Toyao, M. Saito, K. Mochizuki, M. Iwata, H. Higashimura, M. Anpo, M. Matsuoka, J. Phys. Chem. C 116 (2012) 20848–20853.
[35] Y.K. Park, S.B. Choi, H.J. Nam, D.-Y. Jung, H.C. Ahn, K. Choi, H. Furukawa, J. Kim, Chem. Commun. 46 (2010) 3086–3088.
[36] P.W. Du, J. Schneider, P. Jarosz, R. Eisenberg, J. Am. Chem. Soc. 128 (2006) 7726–7727.
[37] W. Zhang, J. Hong, J. Zheng, Z. Huang, J. Zhou, R. Xu, J. Am. Chem. Soc. 133 (2011) 20680–20683.
[38] L. Ma, X. Kang, S. Hu, F. Wang, J. Mol. Catal. (China) 29 (2015) 359–368.
[39] P. Zhang, M. Wang, C. Li, X. Li, J. Dong, L. Sun, Chem. Commun. 46 (2010) 8806–8808.
[40] P.W. Du, R. Eisenberg, Energy Environ. Sci. 5 (2012) 6012–6021.

[41] J.H. Yum, S.R. Jang, P. Walter, T. Geiger, F. Nüesch, S. Kim, J. Ko, M. Grätzel, M.K. Nazeeruddin, Chem. Commun. (2007) 4680–4682.
[42] C. Kong, S. Min, G. Lu, ACS Catal. 4 (2014) 2763–2769.
[43] W. Zhen, B. Li, G. Lu, J. Ma, Chem. Commun. 51 (2015) 1728–1731.
[44] A.P. LaGrow, B. Ingham, S. Cheong, G.V.M. Williams, C. Dotzler, M.F. Toney, D.A. Jefferson, E.C. Corbos, P.T. Bishop, J. Cookson, R.D. Tilley, J. Am. Chem. Soc. 134 (2012) 855–858.
[45] Y. Leng, Y. Li, X. Li, S. Takahashi, J. Phys. Chem. C 111 (2007) 6630–6633.
[46] S. Carenco, C. Boissière, L. Nicole, C. Sanchez, P.L. Floch, N. Mézailles, Chem. Mater. 22 (2010) 1340–1349.
[47] E. Cui, G. Lu, J. Phys. Chem. C 117 (2013) 26415–26425.
[48] J. Liu, C. Li, F. Wang, S. He, H. Chen, Y. Zhao, M. Wei, D.G. Evans, X. Duan, Catal. Sci. Technol. 3 (2013) 2627–2633.
[49] H. Zhang, G. Wu, X. Chen, X. Qiu, Mater. Res. Bull. 41 (2006) 495–501.
[50] J. Li, S. Cheng, Q. Zhao, P. Long, J. Dong, Int. J. Hydrogen Energy 34 (2009) 1377–1382.
[51] L. He, Y. Liu, J. Liu, Y. Xiong, J. Zheng, Y. Liu, Z. Tang, Angew. Chem. Int. Ed. 52 (2013) 3741–3745.
[52] L. Huang, H. Wang, J. Chen, Z. Wang, J. Sun, D. Zhao, Y. Yan, Micropor. Mesopor. Mat. 58 (2003) 105–114.
[53] T.M. Reineke, M. Eddaoudi, M. Fehr, D. Kelley, O.M. Yaghi, J. Am. Chem. Soc. 121 (1999) 1651–1657.
[54] K. Sugikawa, S. Nagata, Y. Furukawa, K. Kokado, K. Sada, Chem. Mater. 25 (2013) 2565–2570.
[55] M. Sabo, A. Henschel, H. Fröde, E. Klemm, S. Kaskel, J. Mater. Chem. 17 (2007) 3827–3832.
[56] H. Li, W. Shi, K. Zhao, H. Li, Y. Bing, P. Cheng, Inorg. Chem. 51 (2012) 9200–9207.
[57] K. Hirai, P. Falcaro, S. Kitagawa, S. Furukawa, Struct. Bond. (Berlin) 157 (2014) 167–186.
[58] Y. Kataoka, K. Sato, Y. Miyazaki, K. Masuda, H. Tanaka, S. Naito, W. Mori, Energy Environ. Sci. 2 (2009) 397–400.
[59] S. Min, G. Lu, J. Phys. Chem. C 115 (2011) 13938–13945.
[60] H. Zhang, X. Lv, Y. Li, Y. Wang, J. Li, ACS Nano 4 (2010) 380–386.
[61] Q. Li, L. Chen, G. Lu, J. Phys. Chem. C 111 (2007) 11494–11499.
[62] D. Li, M.B. Müller, S. Gilje, R.B. Kaner, G.G. Wallace, Nat. Immunol. 3 (2008) 101–105.
[63] D. Tanaka, S. Horike, S. Kitagawa, M. Ohba, M. Hasegawa, Y. Ozawa, K. Toriumi, Chem. Commun. (2007) 3142–3144.
[64] Z. Zhang, S. Xiang, X. Rao, Q. Zheng, F.R. Fronczek, G. Qian, B. Chen, Chem. Commun. 46 (2010) 7205–7207.
[65] T. Lazarides, T. McCormick, P. Du, G. Luo, B. Lindley, R. Eisenberg, J. Am. Chem. Soc. 131 (2009) 9192–9194.
[66] G. Williams, P.V. Kamat, Langmuir 25 (2009) 13869–13873.
[67] H. Ezaki, M. Morinaga, S. Watanabe, Electrochim. Acta 38 (1993) 557–564.
[68] E. Cui, G. Lu, Int. J. Hydrogen Energy 39 (2014) 7672–7685.
[69] J.S. Jang, S.H. Choi, D.H. Kim, J.W. Jang, K.S. Lee, J.S. Lee, J. Phys. Chem. C 113 (2009) 8990–8996.
[70] S.G. Lee, S. Lee, H.I. Lee, Appl. Catal. A: Gen. 207 (2001) 173–181.
[71] D. Wang, M. Gong, H. Chou, C. Pan, H. Chen, Y. Wu, M. Lin, M. Guan, J. Yang, C. Chen, Y. Wang, B. Hwang, C. Chen, H. Dai, J. Am. Chem. Soc. 137 (2015) 1587–1592.